Proceedings of the ASME 2012 Pressure Vessels & Piping Conference
PVP2012
July 15-19, 2012, Toronto, Ontario, CANADA

PVP2012-78075

DESIGN OF UNPARTITIONED, PLUG TYPE HEADER BOXES FOR AIR-COOLED HEAT EXCHANGERS IN REFINERY SERVICE

Hugh-Jean Nel
Sasol Technology
Mechanical & Metallurgical Engineering
Private Bag X1034, Secunda, 2302, Mpumalanga, Republic of South Africa
hugh-jean.nel@sasol.com

Alan Nurick
University of Johannesburg
Department of Mechanical Engineering Science
PO Box 524, Auckland Park, 2006, Gauteng, Republic of South Africa
alann@uj.ac.za

André Leon Nel
University of Johannesburg
Department of Mechanical Engineering Science
PO Box 524, Auckland Park, 2006, Gauteng, Republic of South Africa
andren@uj.ac.za

Francois Lombaard
Sasol Technology
Mechanical & Metallurgical Engineering
Private Bag X1034, Secunda, 2302, Mpumalanga, Republic of South Africa
francois.lombaard@sasol.com

ABSTRACT

Dry air-cooled heat exchangers (ACHE) form an integral part of refinery cooling systems of which the header boxes form an important component. It is commonly designed as an ASME Section VIII Division 1 pressure vessel, but unfortunately neither ASME nor the American Petroleum Institute (API) provide guidance regarding to the methodology which should be used in the assessment of nozzle loads on the header box design. Subsequently, the designer must rely either on empirical guidelines or Finite Element Analysis (FEA) in line with the requirements of ASME Section VIII U-2(g). The aim of this project therefore was to develop an analytical design methodology that accounts for the effects of these nozzle loads on the header box. A new mechanical model was derived by extending the existing ASME Section VIII rigid frame theory model and the result was tested against an FEA case study to determine whether the model was useable. It was found that the new model makes some useful qualitative statements but cannot be used for accurate stress analysis of the stresses near the base of the nozzle on the header box. The case study was also used to examine the effectiveness of a commonly used empirical guideline.

Keywords: Air-cooled Heat Exchanger, Rectangular Pressure Vessel, Nozzle Loading

INTRODUCTION

Dry ACHE are a critical part of refinery cooling systems, especially in arid environments where the amount of cooling water available is restricted. A typical refinery service ACHE, Fig. 1 [1], consists of the tube bank, the fan, motor and drive system, the plenum chamber and the header boxes. The header boxes distribute the inlet flow into the tube bank and collect the outlet flow. Plug-type header boxes are rectangular pressure vessels and are commonly designed according to ASME Section VIII Division 1 Appendix 13 [2] and API 661 [3]. Figure 2 shows the current Appendix 13 [2] model used for the design of unpartitioned, plug-type header boxes. API 661 Section 7.1.10 [3] requires the designer to consider the effects of specified maximum nozzle forces and moments, Fig 3, on the stresses in both the header box and nozzle but gives no guidelines on how this should be done. This has resulted in the use of empirical guidelines or FEA to account for the effects of the nozzle loads. Both approaches have their limitations and the aim of this project was to develop an analytical design methodology that could be used to account for the nozzle loads and allow for a more accurate design without the use of a full FEA investigation.

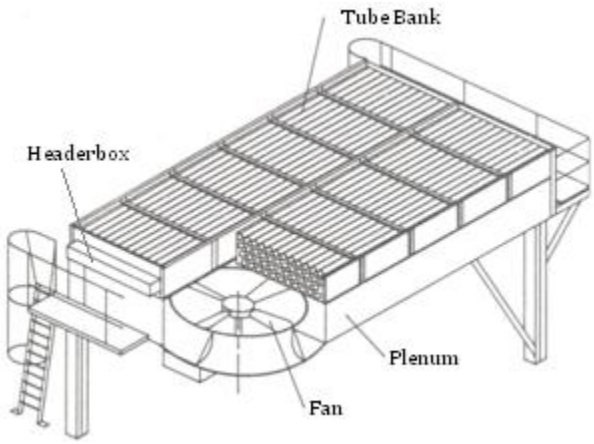

FIGURE 1: TYPICAL REFINERY SERVICE ACHE [1]

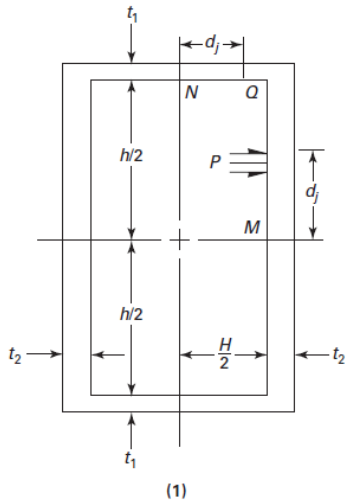

FIGURE 2: CURRENT ASME MODEL [2]

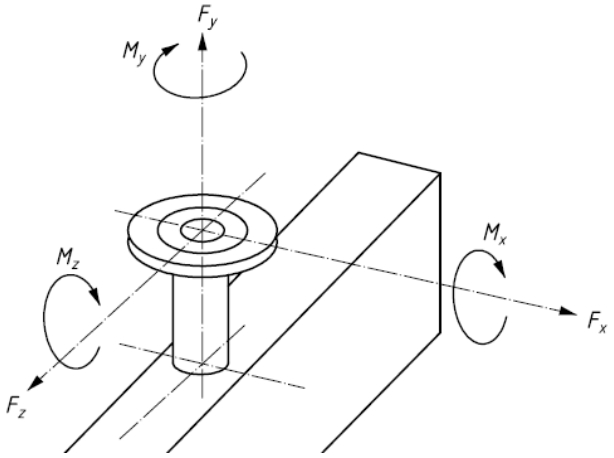

FIGURE 3: DESIGN NOZZLE LOADS [3]

CURRENT DESIGN PRACTICE

Cylindrical and Spherical Vessels

The design of spherical and cylindrical pressure vessels subject to external loading is a well-documented and trusted procedure. The vessel shell can be designed for internal pressure according to UG-27 [2] and the junction reinforcement requirements can be checked using the area method in UG-37 [2] or the pressure-area method of Appendix 1-10 [2]. The stresses in the shell due to the external loadings can be obtained using WRC 107 [4] and the stresses in the nozzle using WRC 297 [5]. The local stresses in both the shell and nozzle may be obtained using WRC 368 [6]. This procedure allows for the safe design of a large proportion of vessel to nozzle junctions that are subject to external loading. If the junction geometry or external loading magnitudes fall outside the applicability criteria of the relevant section then the junction can be designed using FEA and the Design by Analysis rules given in Part 5 of ASME Section VIII Division 2 [7].

Rectangular Vessels

The design of rectangular pressure vessels subject to nozzle loading is far more difficult due to the lack of design guidelines on how to account for these loads. The vessel itself can be designed according Appendix 13 [2] but the reinforcement requirements cannot easily be computed if it is required. This is because neither of the two existing methods for calculating reinforcement requirements in flat heads, UG-39 [2] and Appendix 14 [2], is applicable. Appendix 14 [2] is applicable only to round, flat heads and UG-39 [2] is only applicable to openings which are smaller than half the shortest span, which significantly limits the allowable nozzle size. This is often undesirable in ACHE design as it would force the use of a large number of small nozzles. There is at present no equivalent for WRC 107, 297 and 368 for determining the stresses in rectangular vessels and their attached nozzles. This forces the designer to either use historically proven empirical guidelines or a FEA investigation in line with the requirements of Part 5 of ASME VIII Division 2 [7]. Both of these options have their limitations. The empirical guideline approach is quick to use but only useable for configurations with proven history, making innovation and optimisation very difficult. The FEA investigation route allows for very accurate analysis and complete optimisation but the process is often relatively expensive and lengthy as adequate investigations regarding suitable boundary conditions and loads need to be performed to obtain meaningful results.

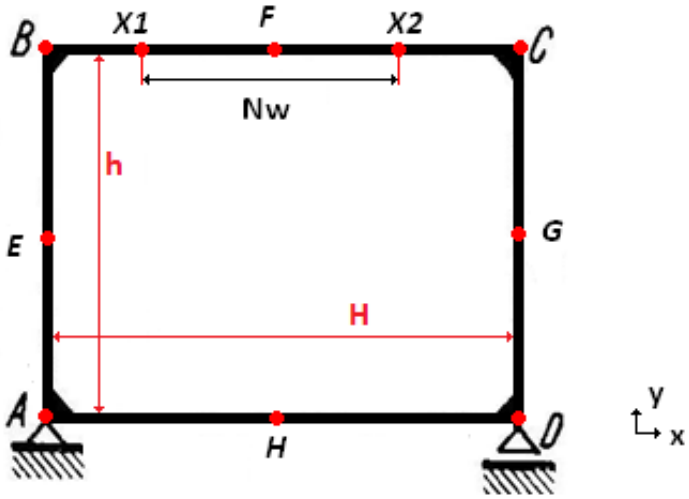

FIGURE 4: VIERENDEEL FRAME

NEW DESIGN METHODOLOGY

Before a new design methodology could be derived, a thorough review of current literature was undertaken so that all possible methods were investigated. Only two possible analytical, closed form techniques were identified: Rigid frame theory, which is used in ASME VIII Division 1 Appendix 13 [2] and Division 2 Part 4.12 [7], and Plate bending theory.

Rigid Frame Theory

Rigid frame theory is an extension of standard beam theory where several beams are rigidly connected together, i.e. there is moment transfer from one beam to another. The model present in Division 1 Appendix 13 [2], Fig. 2, is identical to that in Division 2 Part 4.12 [7] and both work on a unit length basis. This implies that the vessel is assumed to be infinitely long and then a unit section is taken as the basis of the analysis. The effect of this is that the end plates are neglected and only the four side walls remain. This results in a classic rigid frame model, known as the Vierendeel frame [8]. Each of the four walls is modelled as a beam which is rigidly connected to the adjacent sides. Figure 3 depicts the Vierendeel frame at the heart of the Appendix 13 [2] analysis. Furthermore since the only load considered in Appendix 13 [2] is internal pressure, the boundary conditions can be omitted and two axes of symmetry employed, resulting in the simple and easy to use bending and membrane stress equations presented in Appendix 13 [2].This approach becomes increasingly conservative as the overall length of the vessel decreases. Various authors [9-11] have published results clearly indicating the strengthening effect of the end plates. Appendix 13 [2] states that if the ratio of the length to the larger of the width or height is smaller than 4 the rigid frame approach becomes increasingly conservative and also publishes stress reduction factors for length ratios below 2. Zeng [10] claims convergence of the rigid frame approach to a more exact plate bending analysis with length ratios above 5.

Plate Bending Theory

An alternative method for the design of rectangular pressure vessels is to use plate bending theory. This approach was first put forward by Zeng [10] and then refined by Guo [11]. Zeng [10] begins with the same unit length assumption as the Appendix 13 [2] analysis. The double symmetry of the problem is then exploited and this reduces the six walls to two walls, which are then modelled as plates. Each plate is modelled as simply supported and subject to a uniform pressure load and uniformly distributed bending moments along edge where it would be joined to the other plate. The bending moment is there to enforce the condition that at the corners the walls remains perpendicular, i.e. zero relative rotation. The resulting equations are significantly more complex than the rigid frame approach but are still manageable. However for length ratios above 5 these results converge to the rigid frame approach [10]. Guo [11] then extends the approach by considering all six walls and then follows the same approach as before. The resulting system of equations is significantly more complicated than the method of Zeng [10] and offers more accurate results for rectangular vessels of finite length [11]. However these methods results are not exact [11] and do not offer a significant improvement in accuracy for length ratios above 5. The aim of this project is to account for nozzle loading and the application of these loads transforms the 4^{th} order partial differential equation from a linear equation with known solutions to a non-linear equation for which no known closed form solutions could be found [8]. Furthermore Timoshenko [12] states that the omission of these nozzle loads could significantly affect the solutions due to non-linear effects. Finally, the fact that the nozzle hole is usually at least 50% of the width of the top plate will significantly affect the accuracy of both the rigid frame and plate bending approaches.

Extended Rigid Frame Theory

Due to the fact that plate bending theory was not able to yield closed form solutions, rigid frame theory was the only viable method to use to account for the nozzle loading. The rigid frame approach is inherently two dimensional and assumes that the only significant stresses are the bending and membrane stresses in cross-section, as in Fig. 4. Only two of the forces in Fig. 3., F_x and F_y, and one of the moments, M_z, exist in the cross-section and will be considered. The other nozzle loads will be neglected. Since the loading is asymmetric the stress distribution will no longer be symmetric. This means that instead of a single corner point, Q in Fig. 2, and two mid-side points, M and N in Fig. 2, as in the Appendix 13 [2] analysis, each corner and mid-side point will have a unique equation. The loads F_x, F_y and M_z were then applied by distributing them over the entire nozzle width, N_w, in Fig. 4. Bending moment and membrane force equations, Annex A, were then derived using Kleinlogel [13], a classic text on rigid frames. Please note that these equations are not per unit width and that the moment of inertia equations should therefore include vessel length as opposed to the traditional ASME [2] methodology. The stresses at a point can be determined by first following the Appendix 13 [2] approach and determining the pressure related bending and membrane stresses. The stresses induced by the nozzle loads can then be determined by computing the relevant bending moment and membrane force and using standard beam and membrane theory [12] to compute the stresses, which can be algebraically summed with the pressure induced stresses. Note that a positive membrane force is tensile and a positive bending moment causes tension on the internal fibres.

Model Predictions and 2D Validation

The extended rigid frame theory model equations in Annex A make two important predictions regarding the effects of the nozzle loads. Firstly, the nozzle loads will typically have the largest impact at the vessel corners and the smallest impact at the mid-sides. Secondly, the nozzle loads will typically induce stresses that negate the pressure induced stresses at corners A and C, Fig. 3, and induce stresses that sum with the pressure induced stresses at corners B and D. Corners B and D are therefore the critical locations as they will see the highest stress. These predictions were then tested in a series of two dimensional FEA studies. The modelling was done in line with the assumptions of Fig. 4, namely: a pinned joint at point A, a roller joint at point D and the loads distributed over the nozzle width, as shown in Fig. 5. A total of 36 different configurations were tested. In these studies the aspect ratio, α, thickness ratio, TR, and nozzle width ratio, NWR, were varied to ensure that a

large enough sample was taken to test the accuracy of the extended rigid frame model. All FEA studies were tested using 2nd order quadrilateral elements and underwent mesh refinement until the stress values converged to within 3% and the recovered bending moments to within 1%.

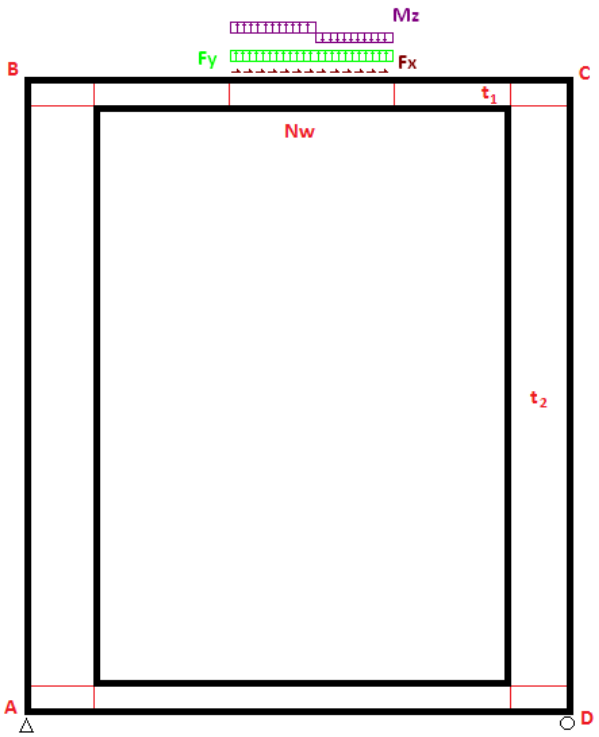

FIGURE 5:2D VALIDATION MODEL SCHEMATIC

Bending moments and tensile forces were recovered from the stress tensors using the method outlined in Annex 5-A in Division 2 [7]. Bending moments and membrane forces were recovered at all mid-side locations as well as points X_1 and X_2 in Fig. 4, which signify the edges of the nozzle. Bending moments and membrane forces were not recovered at the corners, due to the stress concentration effects and a higher order corner effect which will be discussed later, but rather a small distance, 1% of h or H, as applicable, away so as to allow for a more meaningful comparison. These near corner values were then compared to a set of predictive equations designed to predict the values at these points [8].The recovered bending moments were on average within 9% of the values predicted at all locations. The recovered bending moments were also never more than 11.5% larger than the predicted values. The predicted stress values were on average within 13.1% of the FEA results near the corners and within 5.5% at the mid-sides. The larger difference is attributed both to the stress concentration at the corner and a discrepancy with standard beam theory. Based on standard beam theory [12] and the extended rigid frame model predictions the maximum stress should occur at the corners or the mid-sides, depending on vessel geometry. However it was found for all cases examined that near the corners, the maximum external stress was always found a small distance away from the corners and in a different cross-section to that containing the maximum internal stress. Figure 6 shows an enlarged section of corner A for a case where the maximum tensile stress occurs at the sharp corner and the maximum compressive stress occurs a small distance away, at the red line. It is thought that this effect can be attributed to a difference between the way the 2D FEA model, as per Fig. 2 and Fig. 5, and the extended rigid frame model handle the corner joint. Since rigid frame theory is essentially beam theory, the walls are modelled as their mid-planes, which creates an overlap region and a region with no material, while the 2D FEA models the corner completely. This difference in modelling is shown in Fig. 7. The results of the 2D comparison indicate that the extended rigid frame model does predict the 2D behaviour reasonably accurately and could possibly be used as a full design methodology.

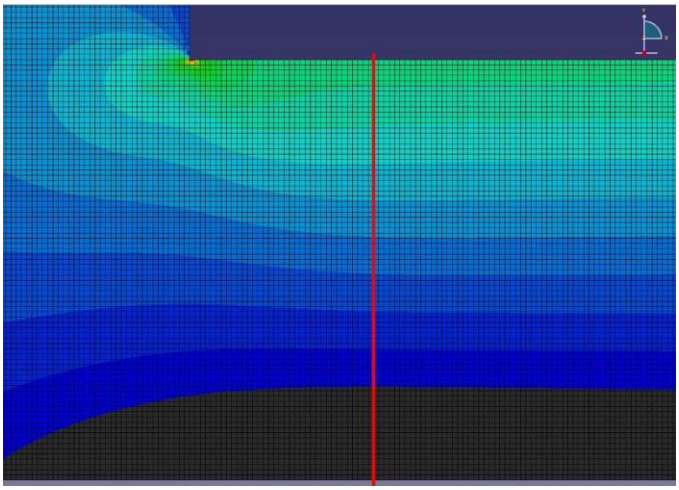

FIGURE 6: MAXIMUM COMPRESSIVE STRESS LOCATION

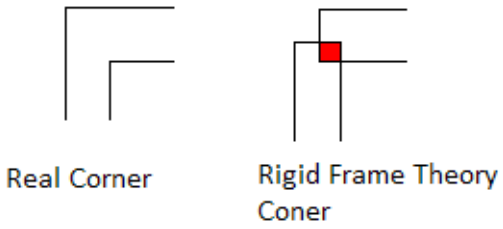

FIGURE 7: COMPARISON OF CORNER MODELLING

FEA CASE STUDY

As a result of the relatively good results in the 2D comparisons it was decided to test the extended rigid frame model on a full 3D specimen using FEA. The specimen used is shown in Fig. 8 and was chosen to match an experimental specimen planned for a later investigation. The dimensions of the specimen were selected to be close to those found in industry and the major dimensions are given in Table 1. The vessel end plates were deliberately omitted as their effect is well known and documented and making the vessel sufficiently

long to remove the end effects leads to both a very large mesh and an expensive and unwieldy experimental specimen. Furthermore this approach is in line with the unit length assumption used in Appendix 13 [2]. For this specific geometry, loaded with the maximum nozzle loads as per API 661 [3], the extended rigid frame model makes two important predictions. Firstly, at corners B and D an external compressive stress is expected and an external tensile stress at corners A and C. Secondly, at the bases of the nozzles an external tensile stress is expected at X_1, near corner B, and an external compressive stress at X_2, near corner C.

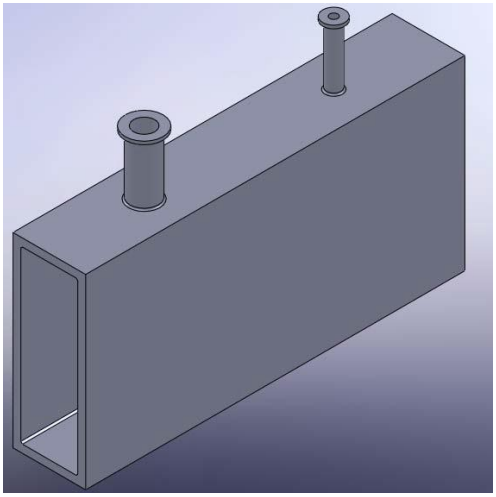

FIGURE 8: 3D FEA MODEL

TABLE 1: 3D FEA MODEL DATA

Aspect Ratio	1/3
h	540 mm
All Wall Thicknesses	25 mm
Large Nozzle	2 ½" WN, at 75% Vessel Length
Small Nozzle	1" LWN, at 25% Vessel Length
Vessel Length	1.2 m

This specimen allows for the effects of a single, externally loaded nozzle on the header box structure as well as the effects of interaction between different nozzles with different loads and sizes. Seven different load cases were considered and the details are given in Table 2. Each nozzle was loaded with the maximum nozzle loads as per API 661 [3] in either the positive direction as in Fig. 3, denoted (+), or the negative direction, (-). This would show how the effects of the nozzle loads interact. For the first five load cases both the full set of six loads and another case with only the planar loads were considered. This would highlight the effect of neglecting the out of plane loads. Load case 6 and 7 would give an indication of the pressure induced stresses and the comparative effect of the nozzle loads. The nozzle loads were applied as distributed pressure loads and surface tractions to the tops of the nozzles, in line with Fig. 3. This means the M_z used in the extended rigid frame model was increased to include the contribution of F_x and the nozzle height.

TABLE 2: LOAD CASES

Load Case	Small Nozzle	Large Nozzle	Pressure
1	1xAPI, (+)	1xAPI, (+)	None
2	1xAPI, (-)	1xAPI, (-)	None
3	1xAPI, (+)	None	None
4	None	1xAPI, (+)	None
5	1xAPI, (-)	1xAPI, (+)	None
6	None	None	250 kPa
7	1xAPI, (+)	1xAPI, (+)	250 kPa

The model was built in ABAQUS and meshed using second order hexahedral elements and convergence was achieved by examining three distinct mesh sizes at 64 points spaced throughout the model and comparing the entire stress tensor. At the finest mesh, 1.2 million elements, the convergence level was 2%. The bending moments and membrane forces at the nozzle bases, points X_1 and X_2 in Fig. 4, were also tested for convergence and they were found to have converged within 1% at the finest mesh. The boundary conditions for the model were identical to the 2D model, corner edge A is free to rotate in the XY plane but not translate while corner edge D is allowed to rotate in the XY plane and translate in the X direction but not in the Y direction. The material has an Elasticity modulus of 200 GPa and a Poisson's ratio of 0.3. An elastic-perfectly plastic model was used with a yield stress of 260 MPa, however in none of the load cases was plasticity encountered.

The results of the first five load cases showed the same general trend. The extended rigid frame model was able to qualitatively predict important trends in the results but was not able to accurately predict the stresses close to the nozzle or away from it. Figure 9 shows the global σ_{xx} contours for load case 1. The σ_{xx} stress component contains the bending and membrane stresses for the top and bottom plate while the σ_{yy} component contains the bending and membrane stresses for the tubesheet and plugsheet. It is important to realise that the Appendix 13 [2] methodology predicts the σ_{xx} and σ_{yy} components in the respective walls and all predictions should be compared to these components as well as the Von Mises stress to determine their accuracy. A close examination of Fig. 9 shows the two main extended rigid frame models predictions for this geometry are present. There are external compressive stress bands at corners B and D and external tensile bands at corners A and C. Furthermore the stresses at X_1 are tensile and compressive at X_2 for both nozzles. Figure 10 shows an enlarged section of the nozzle base and highlights how quickly the stresses dissipate on either side of the nozzle. The results from all load cases showed the local high stresses at the nozzle base dissipate within one nozzle diameter on either side of the nozzle base. However, in contrast to the predictions of the extended rigid frame model, the stress bands at the corners exhibit significant variation along the vessel length. Furthermore the predictions of the extended rigid frame model compare poorly against the FEA results, especially near the nozzle bases. The recovered bending moments and membrane

forces and linearised σ_{xx} and σ_{yy} components for the first five load cases often differed from the predicted values by more than ±800%. The stress linearisation was done using the approach of Annex 5-A in Division 2 [7] and was used to remove the peak stress components, present around structural discontinuities such as the nozzle and corner welds, and leave the membrane and bending stress components, which can be compared to predicted values. It is also worth noting that rigid frame theory predicts a uniform membrane force throughout a wall but the FEA results for all five load cases indicate membrane forces which vary not only with vessel length but throughout the wall. These results indicate that while the extended rigid frame model can make useful qualitative statements about the effects of the nozzle loads, the model is not suitable to accurately predict the resulting stress field. One reason for the poor quality of the predictions lies with the inherent 2D assumption of the extended rigid frame model. The model assumes the nozzle loads are applied via a rectangular area that is N_w wide along the entire length of the vessel. In reality the loads are applied to the header box via the relatively small areas of the nozzle bases, which not constant along vessel length. To accurately capture this, the design methodology would have to be 3D and no suitable 3D, analytical, closed form solution methodology was identified.

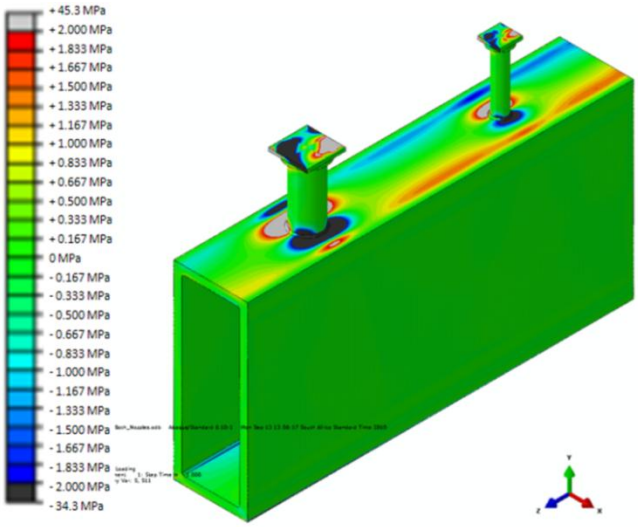

FIGURE 9: GLOBAL σ_{xx} CONTOURS (LC 1)

The next step was to add the effects of internal pressure. Load cases 6 and 7 investigate the effects of internal pressure with and without nozzle loads. Figure 11 and 12 show the global Von Mises contours with 250 kPa internal pressure and 250 kPa and nozzle loads respectively. Both figures show results that are more in line with the rigid frame model predictions and show far less variation along the vessel's length. It is also immediately apparent that the contribution of the nozzle loads is very small compared to that of the internal pressure. Figure 13 and 14 show enlarged sections of the large nozzle base and while the nozzles show differing Von Mises contours, the header boxes themselves show very similar Von Mises contours. The same trends are apparent in Fig. 15 and 16 which show the σ_{xx} contours at the large nozzle bases. It is important to note that in contrast to Fig. 10 the external surface of the top plate in Fig. 16 is entirely in compression, highlighting that the internal pressure creates far larger stresses than the nozzle loads and that the important locations for this geometry will be those where the nozzle loads cause external compressive stresses which will sum with the pressure induced stresses. The predicted stresses also compared far more accurately for both load cases 6 and 7. For load case 6 the predicted stress was on average 8.5% lower than the linearised FEA σ_{xx} and σ_{yy} components and 1% higher than the linearised Von Mises stress at the measured locations. The results for load case 7 show that the percentage difference between the predicted stress and the linearised FEA σ_{xx} and σ_{yy} components decreased to 7.3% while the percentage difference with the linearised Von Mises stresses increased to 1.8%. These results indicate that while the extended rigid frame model cannot be used to make accurate statements about the effects of nozzle loads, the Appendix 13 [2] approach can be used to account for the effects of pressure with good accuracy within the limits presented in Appendix 13 [2]. The results also indicate how small the effects of the maximum API 661 [3] nozzle loads for this geometry's nozzle sizes are compared to the effects of a relatively low internal pressure. In industry header boxes are often designed to withstand internal pressures of 5 MPa. The reason the pressure predictions of the rigid frame model are more accurate is that the pressure loading is constant along the vessel length and as such fits the 2D assumption implicit in the method.

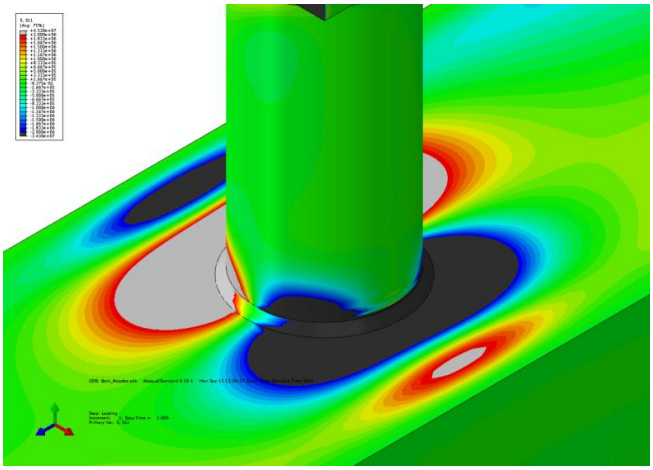

FIGURE 10: σ_{xx} CONTOURS AT LARGE NOZZLE BASE (LC 1)

Finally, a commonly used empirical guideline was tested to see how conservatively it accounted for the effects of nozzle loads. The guideline is to use the standard Appendix 13 [2] design calculations but use a ligament efficiency of 0.5 when calculating the stresses in the top and bottom plate. This effectively doubles the stresses in these plates compared to the case where they have no openings. The nozzle loads transferred

to the header box are then allowed to increase to twice the API 661 [3] maximum nozzle loads. This effectively means that the nozzle loads are allowed to induce maximum stresses as large as those induced by pressure before the vessel will see higher stresses than those it was designed for. This guideline was tested on this geometry by examining the stresses at three points of failure. These locations were the X_2 points at the bases of the large and small nozzle and the highest stress point along corner B. These locations were selected as they represent points where the nozzle loads induce stresses which will sum with those induced by the internal pressure. The nozzle loads were increased until the induced, linearised stresses equal to those induced by the internal pressure at the same location. The nozzle loads were then rounded down to the nearest integer multiple of the API 661 [3] maximum loads. The results indicated that three times the API 661 [3] nozzle loads are required to exceed the stress reserve created by the 0.5 ligament efficiency at the X_2 point of the large nozzle base. Six times the API 661 [3] loads were required at the small nozzle base while 13 times the API 661 [3] loads were required along corner B.

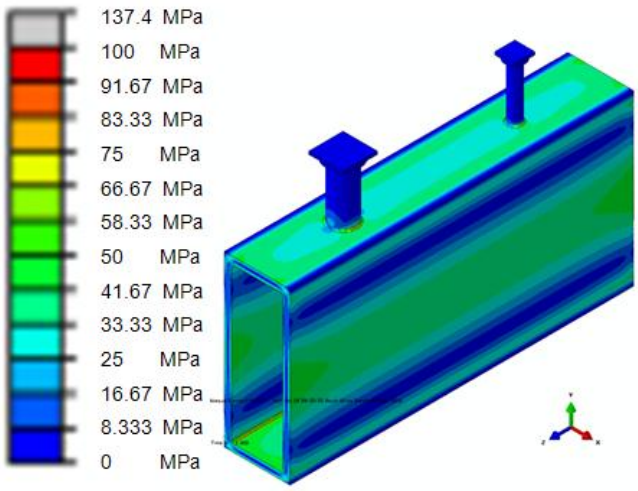

FIGURE 11: GLOBAL VON MISES CONTOURS (LC 6)

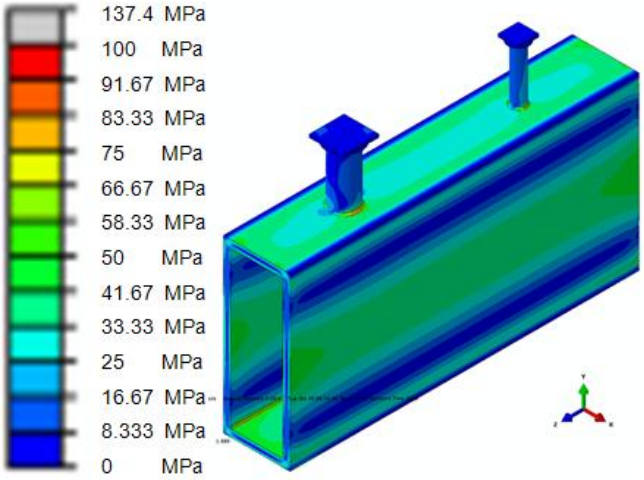

FIGURE 12: GLOBAL VON MISES CONTOURS (LC 7)

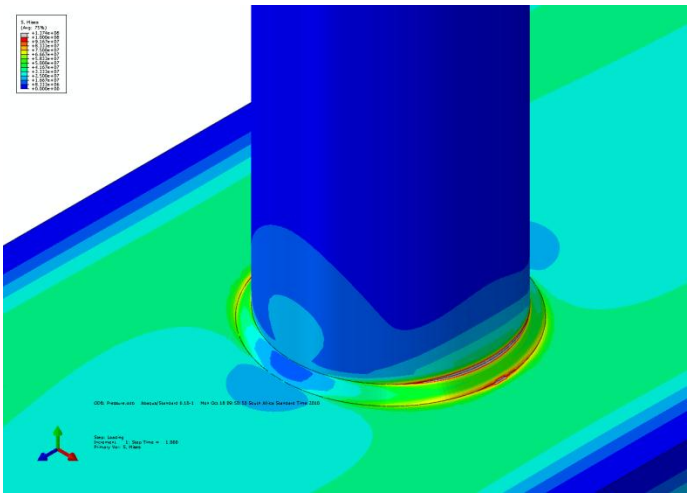

FIGURE 13: VON MISES CONTOURS AT LARGE NOZZLE BASE (LC 6)

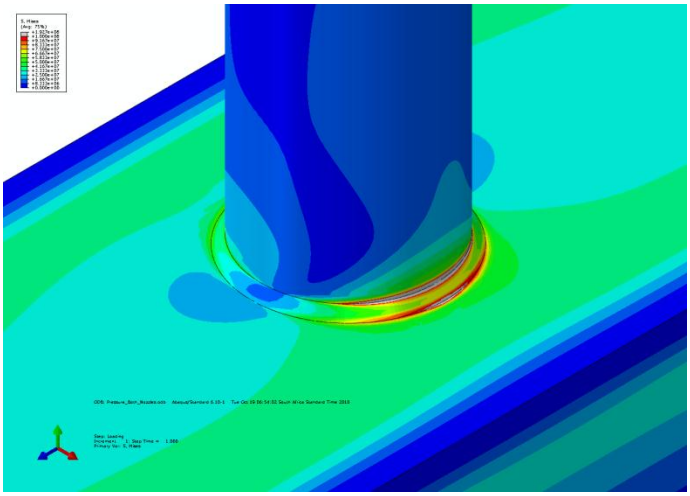

FIGURE 14: VON MISES CONTOURS AT LARGE NOZZLE BASE (LC 7)

The results show that for this geometry the use of the 0.5 ligament efficiency guideline will allow three times the maximum API 661 [3] nozzle loads to be applied to the header box before exceeding the stress reserve. This result is not true in general as it depends on the size of the nozzle and header box as well as the internal pressure. However, while the model header box is fairly representative of the size industrial units, they are subjected to significantly higher internal pressures, and as a result it is thought that the 0.5 ligament efficiency rule will be more conservative as the stress reserve it creates scales linearly with pressure, however more research is required to verify this. Finally the nozzle loads should induce failure at the nozzle to header box junction before failure in the header box itself due to the large stress concentration at the nozzle bases.

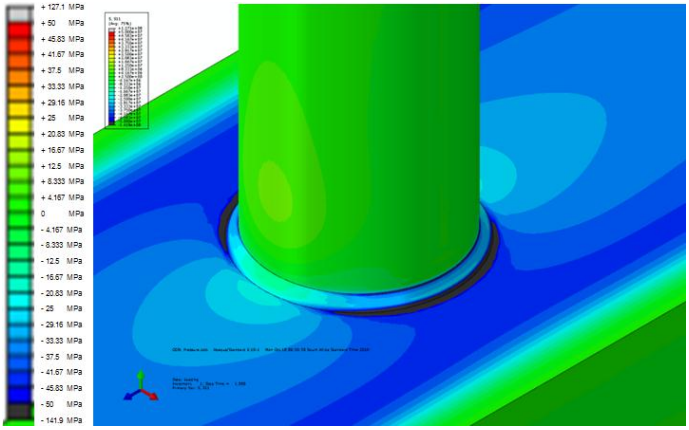

FIGURE 15: σ_{xx} CONTOURS AT LARGE NOZZLE BASE (LC 6)

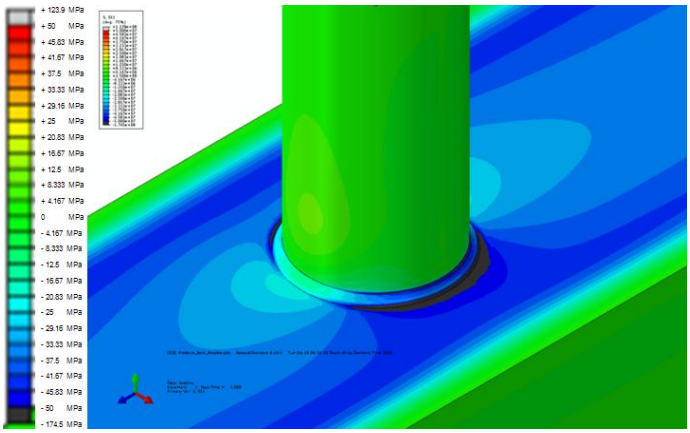

FIGURE 16: σ_{xx} CONTOURS AT LARGE NOZZLE BASE (LC 7)

CONCLUSION

In conclusion the effects of API 661 [3] nozzle loads on unpartitioned, plug type header boxes cannot be accurately predicted by extending the current ASME Section VIII Division 1 Appendix 13 [2] rigid frame theory approach. The existing Appendix 13 [2] closed form methodology can accurately predict the effects of internal pressure, within the limits of Appendix 13 [2], as it does not vary with length and therefore matches the inherent 2D assumptions of the rigid frame model. The nozzle loads however are applied locally and induce stresses which vary significantly along the vessel's length and these effects cannot be accurately predicted using the extended rigid frame model. The extended model can however make some useful qualitative statements about the resulting stress field and where these stresses will sum with those induced by internal pressure. The reported FEA case study examined the conservative nature of a common empirical design guideline, a ligament efficiency of 0.5 for the design of the top and bottom plate, and found it allowed for significantly higher loads than the maximum API 661 [3] to be applied to the header box without causing the vessel to be overstressed. The results further indicate that the guideline could also be conservative for many industrial units although more research will be required to verify this.

NOMENCLATURE

F_x	External Force – X Direction	[N]
F_y	External Force – Y Direction	[N]
F_z	External Force – Z Direction	[N]
H	Vessel Width	[m]
I_1	Moment of Inertia – Horizontal Walls	[m^4]
I_2	Moment of Inertia – Vertical Walls	[m^4]
M	Bending Moment	[Nm]
M_x	External Moment – About X Axis	[Nm]
M_y	External Moment – About Y Axis	[Nm]
M_z	External Moment – About Z Axis	[Nm]
N_w	Nozzle Width	[m]
h	Vessel Height	[m]
t	Vessel Wall Thickness	[m]
σ	Stress	[Pa]

Subscripts

A	At Location A in Fig. 4
B	At Location B in Fig. 4
C	At Location C in Fig. 4
D	At Location D in Fig. 4
E	At Location E in Fig. 4
F	At Location F in Fig. 4
G	At Location G in Fig. 4
H	At Location H in Fig. 4
X_1	At Location X_1 in Fig. 4
X_2	At Location X_2 in Fig. 4
xx	XX or 11 Component of Stress Tensor
yy	YY or 22 Component of Stress Tensor

Dimensionless Ratios

NWR	Nozzle Width Ratio, = N_w/H
TR	Thickness Ratio, = $t_{ab}/t_{bc} = t_2/t_1$
α	Aspect Ratio, = H/h

REFERENCES

[1] Kröger D.G., 1998, "*Air-cooled Heat Exchangers and Cooling Towers"*, Department of Mechanical Engineering, University of Stellenbosch, South Africa

[2] 2010 ASME Boiler & Pressure Vessel Code, Section VIII, Division 1, 2011a Addenda, 1st July 2011, *"Rules for Construction of Pressure Vessels"*, American Society of Mechanical Engineers, New York

[3] API/ANSI Standard 661, 6th Edition, 2006, "*Air-Cooled Heat Exchangers for General Refinery Service"*, American Petroleum Institute, Washington D.C.

[4] Wichman K.R., Hopper A.G., Mershon J.L., 2002 Update, "*Welding Research Council Bulletin 107: Local Stresses in Spherical and Cylindrical Shells due to External Loadings"*, Welding Research Council, INC, New York

[5] Mershon J.L., Mokhtarian K., Ranjan G.V., Rodabaugh E.C., 1987, "*Welding Research Council Bulletin297: Local Stresses in Spherical and Cylindrical Shells due to External Loadings on Nozzles – Supplement to WRC Bulletin 107 – (Revision 1)"*, Welding Research Council, INC, New York

[6] Mokhtarian K., Endicott J.S., 1991, "*Welding Research Council Bulletin368: Stresses in Intersecting Cylinders Subjected to Pressure"*, Welding Research Council, INC, New York

[7] 2010 ASME Boiler & Pressure Vessel Code, Section VIII, 2011a Addenda, 1st July 2011, *"Rules for Construction of Pressure Vessels, Division 2: Alternate Rules"*, American Society of Mechanical Engineers, New York

[8] Nel H-J., 2011, *"Effect of Nozzle Loads on Unpartitioned, Plug Type Headerboxes"*, Master's Thesis, University of Johannesburg

[9] Blach A.E., Hoa V.S., Kwok, C.K., Ahmed A.K.W, February1990, *"Rectangular Pressure Vessels of Finite Length"*, Transactions of the ASME Journal of Pressure Vessel Technology, **112**, pp 50-56

[10] Zeng Z-J., Guo Y-Z., Gao J-J., 1990, *"A New Mechanical Model for Rectangular Structures Subjected to Internal Pressure",* International Journal of Pressure Vessels and Piping, **42**, pp 237-246

[11] Guo Y-Z., Zeng Z-J., 1997, *"The Six-Plate Analytical Method for Pressure Vessels of Finite Length"*, International Journal of Pressure Vessels and Piping, **74**, pp 1-6

[12] Timoshenko, S., Woinowsky-Krieger, S., 1959,"*Theory of Plates and Shells, 2nd Edition.",* McGraw-Hill: NewYork.

[13] Kleinlogel A., 1981, "*Rigid Frame Formulas, 8th Printing.",* Frederick Ungar Publishing Company: New York

ANNEX A

BENDING MOMENT AND MEMBRANE FORCE EQUATIONS

$$M_A = -\frac{F_x h}{4} - \frac{F_y h\left(3H^2 - N_w{}^2\right) I_1}{8H^2 I_2 \left(\left(\frac{2I_1 h}{I_2 H} + 3\right)^2 - \left(\frac{I_1 h}{I_2 H}\right)^2\right)} + \frac{M_z I_2 \left(2H^2 - N_w{}^2\right)}{16H(3hI_1 + HI_2)} \quad (1)$$

$$M_B = \frac{F_x h}{4} + \frac{F_y \left(3H^2 - N_w{}^2\right)\left(\frac{2I_1 h}{I_2 H} + 3\right)}{8H\left(\left(\frac{2I_1 h}{I_2 H} + 3\right)^2 - \left(\frac{I_1 h}{I_2 H}\right)^2\right)} + \frac{M_z I_2 \left(2H^2 - N_w{}^2\right)}{16H(3hI_1 + HI_2)} \quad (2)$$

$$M_C = -\frac{F_x h}{4} + \frac{F_y \left(3H^2 - N_w{}^2\right)\left(\frac{2I_1 h}{I_2 H} + 3\right)}{8H\left(\left(\frac{2I_1 h}{I_2 H} + 3\right)^2 - \left(\frac{I_1 h}{I_2 H}\right)^2\right)} - \frac{M_z I_2 \left(2H^2 - N_w{}^2\right)}{16H(3hI_1 + HI_2)} \quad (3)$$

$$M_D = \frac{F_x h}{4} - \frac{F_y h\left(3H^2 - N_w{}^2\right) I_1}{8H^2 I_2 \left(\left(\frac{2I_1 h}{I_2 H} + 3\right)^2 - \left(\frac{I_1 h}{I_2 H}\right)^2\right)} - \frac{M_z I_2 \left(2H^2 - N_w{}^2\right)}{16H(3hI_1 + HI_2)} \quad (4)$$

$$M_E = -\frac{F_y h\left(3H^2 - N_w{}^2\right) I_1}{16H^2 I_2 \left(\left(\frac{2I_1 h}{I_2 H} + 3\right)^2 - \left(\frac{I_1 h}{I_2 H}\right)^2\right)} + \frac{F_y \left(3H^2 - N_w{}^2\right)\left(\frac{2I_1 h}{I_2 H} + 3\right)}{16H\left(\left(\frac{2I_1 h}{I_2 H} + 3\right)^2 - \left(\frac{I_1 h}{I_2 H}\right)^2\right)} + \frac{M_z I_2 \left(2H^2 - N_w{}^2\right)}{16H(3hI_1 + HI_2)} \quad (5)$$

$$M_F = -\frac{F_y (2H - N_w)}{8} + \frac{F_y \left(3H^2 - N_w{}^2\right)\left(\frac{2I_1 h}{I_2 H} + 3\right)}{8H\left(\left(\frac{2I_1 h}{I_2 H} + 3\right)^2 - \left(\frac{I_1 h}{I_2 H}\right)^2\right)} - \frac{M_z I_2 \left(2H^2 - N_w{}^2\right)}{16H(3hI_1 + HI_2)} \quad (6)$$

$$M_G = -\frac{F_y h\left(3H^2 - N_w{}^2\right) I_1}{16H^2 I_2 \left(\left(\frac{2I_1 h}{I_2 H} + 3\right)^2 - \left(\frac{I_1 h}{I_2 H}\right)^2\right)} + \frac{F_y \left(3H^2 - N_w{}^2\right)\left(\frac{2I_1 h}{I_2 H} + 3\right)}{16H\left(\left(\frac{2I_1 h}{I_2 H} + 3\right)^2 - \left(\frac{I_1 h}{I_2 H}\right)^2\right)} - \frac{M_z I_2 \left(2H^2 - N_w{}^2\right)}{16H(3hI_1 + HI_2)} \quad (7)$$

$$M_H = -\frac{F_y h\left(3H^2 - N_w{}^2\right) I_1}{8H^2 I_2 \left(\left(\frac{2I_1 h}{I_2 H} + 3\right)^2 - \left(\frac{I_1 h}{I_2 H}\right)^2\right)} \quad (8)$$

$$M_{X_1} = \frac{F_x h N_w}{4H} - \frac{F_y (H - N_w)}{4} + \frac{F_y \left(3H^2 - N_w{}^2\right)\left(\frac{2I_1 h}{I_2 H} + 3\right)}{8H\left(\left(\frac{2I_1 h}{I_2 H} + 3\right)^2 - \left(\frac{I_1 h}{I_2 H}\right)^2\right)} - \frac{M_z (H - N_w)}{2H} + \frac{M_z I_2 \left(2H^2 - N_w{}^2\right)}{16H(3hI_1 + HI_2)} \quad (9)$$

$$M_{X_2} = -\frac{F_x h N_w}{4H} - \frac{F_y (H - N_w)}{4} + \frac{F_y \left(3H^2 - N_w{}^2\right)\left(\frac{2I_1 h}{I_2 H} + 3\right)}{8H\left(\left(\frac{2I_1 h}{I_2 H} + 3\right)^2 - \left(\frac{I_1 h}{I_2 H}\right)^2\right)} + \frac{M_z (H - N_w)}{2H} - \frac{M_z I_2 \left(2H^2 - N_w{}^2\right)}{16H(3hI_1 + HI_2)} \quad (10)$$

$$N_{AD} = \frac{F_x}{2} + \frac{F_y I_2 \left(N_w{}^2 - 3H^2\right)}{8h(I_1 h + 3I_2 H)} \quad (11)$$

$$N_{AB} = \frac{F_y}{2} + \frac{F_x h}{2H} + \frac{M_z \left(10 I_2 H^2 + 24 h H I_1 - I_2 N_w{}^2\right)}{8H^2 (I_2 H + 3I_1 h)} \quad (12)$$

$$N_{BC} = \frac{-F_x}{2} - \frac{F_y I_2 \left(N_w{}^2 - 3H^2\right)}{8h(I_1 h + 3I_2 H)} \quad (13)$$

$$N_{CD} = \frac{F_y}{2} - \frac{F_x h}{2H} - \frac{M_z \left(10 I_2 H^2 + 24 h H I_1 - I_2 N_w{}^2\right)}{8H^2 (I_2 H + 3I_1 h)} \quad (14)$$